Solvation and Solvatochromism in CO 2 - Expanded Liquids. 2. Experiment−Simulation Comparisons of Preferential Solvation in Three Prototypical Mixtures

ARTICLE *in* THE JOURNAL OF PHYSICAL CHEMISTRY B · APRIL 2007

Impact Factor: 3.3 · DOI: 10.1021/jp067916y · Source: PubMed

3 AUTHORS, INCLUDING:

Mark Maroncelli
Pennsylvania State University
126 PUBLICATIONS **11,711** CITATIONS

SEE PROFILE

Solvation and Solvatochromism in CO_2-Expanded Liquids. 2. Experiment−Simulation Comparisons of Preferential Solvation in Three Prototypical Mixtures

Hongping Li,† Sergei Arzhantsev, and Mark Maroncelli*

Department of Chemistry, The Pennsylvania State University, 104 Chemistry Building, University Park, Pennsylvania 16802

Received: November 29, 2006; In Final Form: January 15, 2007

Electronic absorption and emission spectra of 10-bis(phenylethynyl)anthracene (PEA) and coumarin 153 (C153) are measured as functions of composition along the bubble-point curve at 25 °C in CO_2-expanded cyclohexane (c-C_6H_{12}), acetonitrile (CH_3CN), and methanol (CH_3OH). The nonlinear dependence of the spectral frequencies on composition suggests substantial preferential solvation of both solutes by the liquid components of these mixtures. Estimates of enrichment factors (local mole fraction of a component divided by its bulk value) based on the assumption that spectral shifts are linearly related to local composition are quite large (∼10) in the cases of the C153/CH_3CN + CO_2 and C153/CH_3OH + CO_2 systems at high x_{CO_2}. Computer simulations of anthracene, the chromophore of PEA, and C153 in these three CO_2-expanded liquids are used to clarify the relationship between local composition and spectral shift. A semiempirical model consisting of additive electrostatic and dispersive interactions is able to capture the main features observed experimentally in all six solute/solvent combinations. The simulations show that the commonly used assumption of a linear relation between spectral shifts and local compositions grossly exaggerates the extent of preferential solvation in these mixtures. The collective nature of electrostatic solvation and the composition dependence of the solute's coordination number are shown to be responsible for the breakdown of this assumption.

1. Introduction

Gas-expanded liquids (GXLs) are mixtures consisting of a liquid organic solvent and a near-critical gas such as CO_2. These mixtures are currently being explored as potential replacements for pure organic solvents in chemical processing.[1−4] As such, they reflect a compromise between the use of conventional solvents, which are a major source of industrial pollution, and the completely benign solvent CO_2, whose poor solvent qualities and high pressure requirements have limited its application. In addition to the environmental benefits of GXLs, the ability to readily pressure tune the mole fraction of the gaseous component and thereby alter the solvating power, fluidity, and many other properties of these solvents proves advantageous in a variety of applications, such as materials processing,[5,6] analytical separations,[7] and cleaning,[8] and as media for organic reactions.[2,9,10] Despite the interest in applications, the nature of solvation in GXLs has not been fully characterized. Available data on solvation primarily consists of measurements of solubilities of organic solids studied in relation to the use of CO_2 in gas−antisolvent particle processing.[11,12] Molecular aspects of solvation, for example, the composition of the local environment surrounding a solute and how it might differ from that in the bulk solvent, remain relatively little explored.[3]

Spectroscopic measurements provide perhaps the simplest experimental approach for learning about the local environment of a solute.[13,14] A few studies have already used the electronic absorption spectra of solvatochromic probes[3,15−17] or analogous vibrational measurements[18,19] to examine solvation in GXLs. In a pioneering study, Kim and Johnston[15] monitored shifts of the visible absorbing dye phenol blue in four supercritical CO_2 + liquid solvent mixtures over wide ranges of composition and pressure. By making some simple assumptions about how spectral shifts depend on local composition, they determined local mole fractions of the two solvent components in the cybotactic region and reported that at low liquid-component mole fractions (1−2%) and at low pressures (8−10 MPa) there is a 5−10-fold enrichment of the liquid component in the neighborhood of the solute. A number of later investigations into the effect of dilute entrainers on supercritical solvation also reported very large enrichments using similar spectroscopic methods.[20−24] Kelley and Lemert[16] were the first to measure solvatochromism in GXLs under conditions of liquid−vapor coexistence. Using the same phenol blue probe and analysis methods as Kim and Johnston,[15] Kelley and Lemert determined local compositions about phenol blue in mixtures of CO_2 + cyclohexane, toluene, tetrahydrofuran, acetone, and methanol at mole fractions up to 95% in CO_2. Similarly to what was found under supercritical conditions, Kelley and Lemert reported enrichment factors of 5−10 in the liquid component at high CO_2 dilutions along the coexistence curve. Most recently, Eckert and co-workers[17] measured absorption shifts of several probe solutes to characterize the π^*, α, and β solvatochromic parameters[25,26] of CO_2 + acetone and methanol mixtures. In the case of the CO_2 + methanol system, which they later analyzed in terms of local compositions,[3] these workers reported variable enhancements depending on the solute. They reported negligible solvent preference in the case of a betaine solute and up to a 6-fold preference for methanol over CO_2 when 4-nitrophenol was the solute at high x_{CO_2}.

* Author to whom correspondence should be addressed. E-mail: maroncelli@psu.edu.

† Current address: Department of Chemistry, Zhengzhou University, No.100 Science Road, Zhengzhou, Henan 450001, China.

10.1021/jp067916y CCC: $37.00
Published on Web 03/07/2007

CHART 1

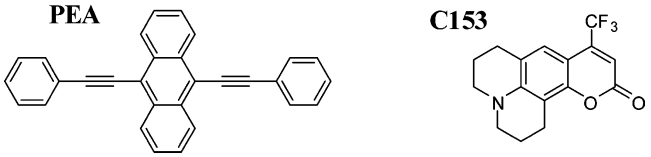

Computer simulations provide an alternative means for exploring molecular aspects of solvation in GXLs, and a number of simulation studies have been performed recently.[27−37] Thus far the systems CO_2 + methanol[27−31,33,35,36] and CO_2 + acetonitrile[32,34,36] have enjoyed the most attention, but more limited simulations of CO_2 + acetone,[35,36] cyclohexane,[36] and a number of other solvents[33,37] have also been performed. Simulations of phase behavior suggest that standard intermolecular potentials previously tuned to reproduce the properties of the neat component liquids provide reasonably accurate representations of liquid−vapor coexistence in such mixtures.[28,29,31−33] Experimental data on other properties such as dielectric constants, viscosities, and diffusion constants are currently limited, but available comparisons suggest reasonable fidelity is to be expected for such properties as well.[30,34−36] A number of workers have therefore used these same simulations to examine solvation structure in the CO_2 + methanol system[28−31,35,36] and to a lesser extent in other GXLs.[32,35−37] As might be expected, methanol−methanol hydrogen bonding promotes clustering of methanol molecules even at high CO_2 concentrations,[29−31,33,35,36] which leads to a significant preference for methanol molecules in the first solvation shell of a central methanol "solute" in the CO_2 + methanol system.[36] In GXLs in which hydrogen bonding is absent, the preference for liquid-component molecules to be solvated by other liquid-component molecules is still observed, but it is considerably reduced.[36] In general, it appears that the enrichment factors observed in these simulations of CO_2 + a liquid solvent tend to be smaller than the enrichment about the solvatochromic probes measured in experiment. But no direct comparisons between simulations and spectroscopic measurements have yet been reported in GXLs, although one analogous study has been performed of a liquid alkane + alcohol mixture.[38,39]

In the present work we describe such experiment−simulation comparisons, undertaken with the goal of gaining a better understanding of how solvatochromic measurements relate to local compositions in GXLs. Since the work of Kim and Johnston[15] virtually all analyses of solvatochromic data in these mixtures[3,16,20−24] (and in conventional liquid mixtures as well[14]) have relied on the assumption that spectral shifts are linear functions of the composition of the cybotactic region. Especially when polar interactions are involved, the accuracy of this assumption is questionable, and we anticipated that its use might significantly exaggerate the extent of preferential solvation in GXLs. To explore this possibility, we have performed parallel spectroscopic measurements and computer simulations on the two solutes 10-bis(phenylethynyl)anthracene (PEA) and coumarin 153 (C153) shown in Chart 1 in mixtures of CO_2 with the three liquid solvents cyclohexane, acetonitrile, and methanol (hereafter denoted c-C_6H_{12}, CH_3CN, and CH_3OH). The solutes were chosen to provide examples of spectral shifts that mainly result from nonpolar solute−solvent interactions (PEA) and the more common case in which both electrostatic and nonpolar interactions contribute significantly (C153). We measured both absorption and emission spectra so as to monitor local compositions about both the S_0 and the S_1 states of these solutes. The three liquid solvents were chosen to encompass a broad range of interaction types, from nonpolar (c-C_6H_{12}) to highly polar but aprotic (CH_3CN) to strongly associated (CH_3OH). Among the six solute + solvent combinations studied here we therefore expect to include most of the situations likely to be encountered in such experiments.

The simulations reported here employ models of the binary CO_2 + liquid solvent mixtures characterized in a previous paper.[36] To the former systems we now add a single solute molecule representing either C153 or PEA. Because of previous modeling studies[40] as well as for simplicity, we have chosen to simulate anthracene, the primary chromophore in PEA, rather than the PEA molecule itself. As will be shown below, the solvatochromism of anthracene and PEA have similar origins, and this substitution makes little difference to the spectroscopic modeling performed here. To model solvatochromism we employ a very simple semiempirical model based on S_1-S_0 differences in the dispersion and electrostatic interactions between the solute and the surrounding solvent molecules. Although much more sophisticated treatments of the solvatochromism of molecules such as C153 have been described,[41−45] the present approach suffices to approximately reproduce the composition dependence of all of the shifts of a given solute observed experimentally with only a single adjustable parameter. The simplicity of this approach helps to expose important differences in the ways that nonpolar and electrostatic spectral shifts report on the local environment of a solute.

2. Experimental Methods

The probes, coumarin 153 (C153), and 9,10-bis(phenylethynyl)anthracene (PEA) were obtained from Exciton (laser grade) and Aldrich (97%), respectively. Absorption and emission spectra of these probes showed no signs of impurities when used as received. The liquid solvents c-C_6H_{12}, CH_3CN, and CH_3OH were spectrophotometric or HPLC grade (≥99.9%) from Sigma-Aldrich and were used as received. The CO_2 was supercritical fluid extraction (SFE) research grade from Scott Specialty Gases (>99.995%) and was passed through activated charcoal and O_2 traps prior to use.

The spectroscopic cell used for these experiments was a modified version of cells previously used for supercritical fluid experiments.[46,47] The body of the cell is a stainless steel cube with three quartz windows and a filling port arranged in a horizontal plane surrounding a sample volume of ∼4 mL. The path length for absorption measurements is 2.7 cm. A 50 mL stainless steel cylinder was added to the top of this basic cell to accommodate the volume expansion of the GXLs. The entire cube + cylinder composite was immersed in a plexiglass enclosure, and circulating water was used to thermostat the system to 298.2 ± 0.2 K in all of the experiments described here. CO_2 was delivered to the cell using a syringe pump (ISCO 100DM), and pressures were measured using an Omega PX 602 transducer with an accuracy of ±35 kPa. Absorption spectra were recorded using a Hitachi U-3010 UV/vis spectrophotometer, and corrected emission spectra with a Spex Fluorolog F212 fluorimeter.

Samples along the bubble-point curve were prepared by dissolving the amount of solute required to achieve a desired initial absorbance (∼1.5 in absorption and ∼0.2 in emission measurements) in 4 mL of the liquid solvent component. Beginning with this pure liquid sample, a series of spectra were recorded at increasing pressures of CO_2 and a fixed total volume. The compositions of the liquid phase were determined using known relations between the liquid composition and the coexisting vapor pressure. In the cases of CH_3CN + CO_2 and

$CH_3OH + CO_2$ such data are available from literature sources.[48,49] Only limited data are available on the c-$C_6H_{12} + CO_2$ system,[50] and compositions were therefore estimated using the Peng−Robinson equation of state.[51]

Initial experiments showed equilibration to be problematic for the cell geometry employed here, which has a limited gas−liquid surface area for some fill volumes. We found that slow addition of CO_2 by bubbling it through the liquid phase was necessary to provide effective initial mixing. After an addition of CO_2 in this manner, the liquid was stirred for 20−50 min, and the pressure then was allowed to stabilize in the absence of stirring for a comparable period. Typically 1.5 h were allowed between different compositions to ensure equilibration as signaled by steady values of absorption or emission intensities. In the case of absorption measurements, we could use the relative change in absorbance, assuming composition-independent extinction coefficients, to monitor the volume expansion of the liquid phase. Such measurements were within expected uncertainties of the values calculated from volumetric data. To obtain data at very high CO_2 concentrations we also recorded some spectra in the one-phase region by pipetting 20−250 μL of stock solution of the probe in the liquid component and metering in an appropriate volume of CO_2 to provide the desired composition.

3. Simulation Models and Methods

Molecules in this study were modeled as rigid collections of interaction sites with the interactions between sites being of the Lennard-Jones (12−6) plus Coulomb form. The solvent models were united atom representations (CH_2 and CH_3 groups treated as single interaction sites) previously reported in the literature for describing the neat solvents. The CO_2 model was the EPM2 model of Harris and Yung,[52] the model of c-C_6H_{12} was from the OPLS-UA force field,[53] the CH_3CN model was from the work of Edwards et al.,[54] and the CH_3OH model was from Haughney et al.[55] A compilation of the potential parameters as well as a discussion of the performance of these models for describing the properties of GXL mixtures is provided in ref 36.

For the solutes C153 and anthracene (the chromophore of PEA), all-atom representations were used. The geometries, assumed to be the same in the ground and excited electronic states, were taken from optimizations at the RHF/6-31G(d) level of theory. Ground-state solute charges were obtained from electrostatic potential (ESP) fits to the RHF wave function in the case of C153 or to the MP2/6-31G(d) wave function in the case of anthracene. S_1-S_0 charge differences needed for the spectral shift calculations described below were obtained from ESP fits to AM1/CI wave functions. Trajectories run in the presence of the S_1 solute employed charges obtained by adding the AM1 charge differences to the ab initio S_0 charges. The parameters specifying the Lennard-Jones interactions of the solutes were taken from the OPLS-AA force field.[56] A complete listing of solute parameters is provided in Tables S1 and S2 of the Supporting Information. In all cases Lorentz−Berthelot combining rules were used for determining the Lennard-Jones parameters between unlike atoms.

To model solvent-induced shifts, $\Delta\nu = \nu - \nu_{gas}$, we assumed the inhomogeneous broadening limit and calculated $\Delta\nu$ from differences between solute−solvent interaction energies (U) in the S_1 and S_0 states

$$h\Delta\nu_{abs} = \langle \Delta U \rangle_0 \quad \text{and} \quad h\Delta\nu_{em} = \langle \Delta U \rangle_1 \tag{1}$$

where $\Delta U = U(S_1) - U(S_0)$ and $\langle x \rangle_i$ indicates an average over a trajectory in equilibrium with solute state i. In general, one expects contributions to ΔU from changes in short-range repulsion, dispersion, electrostatic, and induction interactions.[57] Motivated by preliminary simulations in neat solvents,[40] we assumed that the spectral shifts of interest here are dominated by independent contributions from dispersion and electrostatic interactions[58]

$$\Delta U = \Delta U_{dsp} + \Delta U_{el} \tag{2}$$

Dispersion interactions were modeled using

$$\Delta U_{dsp} = -\sum_{\alpha}\sum_{j} f_\alpha C_{\alpha j}^{(0)} \quad C_{\alpha j}^{(0)} = 4\epsilon_{\alpha j}\sigma_{\alpha j}^6/r_{\alpha j}^6 \tag{3}$$

where the indices α and j label solute and solvent atoms, respectively, and $\epsilon_{\alpha j}$ and $\sigma_{\alpha j}$ are Lennard-Jones interaction parameters. Equation 3 assumes that S_1-S_0 changes in the dispersion interactions between the solvent and a particular solute atom α are proportional by a factor f_α to the value of this interaction in the S_0 state ($C_{\alpha j}^0$). The factor f_α can be chosen to be the same for all solute atoms involved in the transition or alternatively can be chosen to be proportional to calculated transition densities on the chromophore atoms.[59] In practice, either method provides a reasonable representation of the spectral shifts of anthracene in a variety of solvents with only a single adjustable parameter.[40] Here we assumed f_α to be the same for all atoms in the π system of the solute and is zero elsewhere. In this case, eq 3 reduces to

$$\Delta U_{dsp} = -f\sum_{\alpha'}\sum_{j} C_{\alpha' j}^{(0)} \equiv f U_{dsp} \tag{4}$$

where α' restricts the summation to only the relevant chromophore atoms and f is a constant characteristic of the solute. We note that the approach adopted here can be viewed as a greatly simplified version of the perturbation treatment of dispersion-induced spectral shifts introduced by Shalev et al.[60] and its variants.[59,61] For fluid systems of the sort examined here, such a simplified representation is sufficient to model variations in spectral shifts of nonpolar chromophores as a function of variables such as solvent density[40,59] and composition.[40]

To model the electrostatic contribution we used

$$\Delta U_{el} = \sum_{\alpha}\sum_{j} \frac{\Delta q_\alpha q_j}{r_{\alpha j}} \tag{5}$$

where the Δq_α's are S_1-S_0 differences in effective solute charges and the q_j's are solvent charges. A number of past studies[38,44,62−65] have shown that when charge differences obtained from semiempirical or ab initio wave functions are used for the Δq_α's this electrostatic component alone provides reasonably accurate predictions of the reorganization energies of C153 in a number of solvents.

Simulations were performed using a modified version of the DL_POLY program.[66] The systems simulated consisted of a single solute molecule solvated with 343−1000 solvent molecules. In the case of unmixed solvents, 343 (c-C_6H_{12}), 512 (CH_3CN and CH_3OH), or 1000 (CO_2) molecules were used, whereas for all of the GXL mixtures a total of 1000 solvent molecules was used. Simulations were performed in the NVT ensemble at a temperature of 298 K using a Nosé−Hoover thermostat.[67] System volumes were chosen to provide approximately the densities expected in experiment. To do so a

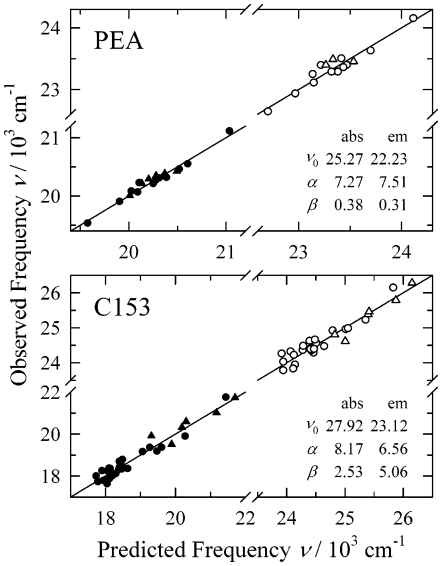

Figure 1. Correlation of absorption (open symbols) and emission frequencies (filled symbols) of PEA and C153 in liquid solvents according to eq 6. Circles denote aprotic solvents, and triangles protic solvents. Data are from refs 47 and 69. (In the case of C153, solvents in refs 47 and 69 having considerable quadrupolar character, which are not amenable to the dielectric representation of eq 6, have not been included.) The number of solvents N and standard error σ in these correlations are as follows (N, σ/10^3 cm^{-1}): PEA absorption (14, 0.11), PEA emission (18, 0.06), C153 absorption (30, 0.18), and C153 emission (30, 0.27).

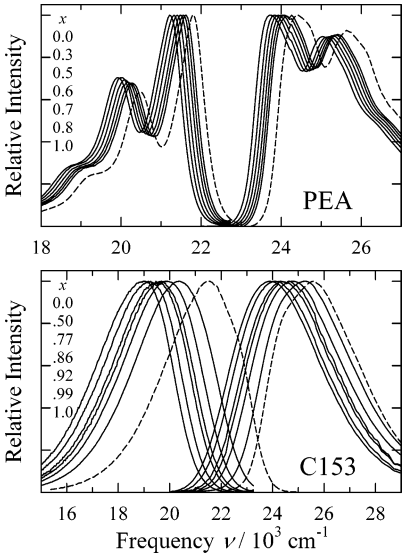

Figure 2. Absorption and emission spectra of PEA (top panel) and C153 (bottom panel) in CH_3CN + CO_2 mixtures. Spectra shift from low to high frequency with increasing CO_2 concentration. Approximate values of x_{CO_2} are indicated. Spectra in neat CO_2 (6.5 MPa) are shown as dashed lines. For clarity, all of the absorption spectra of PEA have been shifted by +2000 cm^{-1}.

constant volume of 205 cm^3/mol was added to the volumes corresponding to experimental densities of the liquid mixtures in the absence of the solute (see ref 36). This additional volume was determined from the partial molar volumes of the solutes observed in NPT simulations of the neat liquid solvents.[68] Cubic periodic boundary conditions were applied, and long-range interactions were treated using the standard Ewald method. Rigid body equations of motion were integrated using a leapfrog scheme with a 2 fs time step. After insertion of the solute into a pre-equilibrated solvent mixture, the systems were equilibrated for at least 500 ps prior to data collection. Trajectory data were collected over 1−2 ns in 200 ps blocks, and the blocks were averaged to obtain estimates of statistical uncertainties (standard errors of the mean) in the results reported.

4. Experimental Solvatochromism

The two solutes employed in this study were chosen to represent cases in which spectral shifts are dominated by nonpolar interactions (PEA) as well as the more typical case wherein both nonpolar and electrostatic interactions are important (C153). Figure 1 illustrates the different characteristics of the solvatochromism of these probes by showing correlations of previously reported data in conventional liquid solvents[47,69] using the relation

$$\nu = \nu_0 - \alpha f(n_D^2) - \beta\{f(\epsilon_r) - f(n_D^2)\} \quad \text{with} \quad f(x) = \frac{x-1}{x+2} \tag{6}$$

where n_D denotes the refractive index and ϵ_r the relative permittivity of the solvent.[70] The coefficient α in this expression is a measure of the sensitivity of the spectral frequency to the solvent electronic polarizability whereas the coefficient β measures the sensitivity to "nuclear" solvent polarizability, or that portion of the solvent response that results from interactions with the permanent charge moments of solvent molecules. These data show that electronic shifts of PEA respond primarily to a solvent's electronic polarizability. To within the uncertainty of these data (±50 cm^{-1}) no difference is observed between the solvent dependencies of the absorption and emission shifts of PEA; i.e., there is no discernible solvent contribution to its Stokes shift. In C153, however, interactions with both the electronic polarizability and the electrostatic moments of solvent molecules contribute comparably to the spectral shifts. There is also a large difference between the relative contributions of these two terms to the absorption and emission shifts, which results in a large (up to 2300 cm^{-1} [69]) solvent contribution to the C153 Stokes shift.

Spectra of PEA and C153 in CH_3CN + CO_2 are shown in Figure 2. Similar spectra are observed in the two other GXLs studied. The main effect of adding CO_2 to the pure liquid solvent (the redmost spectra) is to simply shift the spectrum to the blue. In the case of PEA, there is little discernible change in the width or shape of the spectra in any of the systems studied.[71] In the case of C153 there are also small systematic changes to the widths of the bands, as signaled, for example, by the appearance of subtle vibronic structure in the neat CO_2 spectra.

To accurately measure frequency shifts and to obtain information about possible width variations, all spectra were fit to an inhomogeneous broadening model. Line shape functions (ν^{-1}-weighted absorption and ν^{-3}-weighted emission spectra) derived from reference spectra in 2-methylbutane (2MB) were shifted and convoluted with a Gaussian broadening function to fit the experimental spectra using a least-squares algorithm. Two examples of this type of fitting are shown in Figure 3, which illustrates data from the C153/c-C_6H_{12} + CO_2 system. The spectra of C153 are most structured in c-C_6H_{12} and CO_2, and for this reason the fits displayed here are among the least accurate. Nevertheless, such fits provide estimates of relative frequency shifts that are reproducible to ±30 cm^{-1} as well as reasonable measures of the solvent-induced broadening of the spectra. Parameters of these fits for all of the systems studied are compiled in Table S3 of the Supporting Information.

Spectral frequencies determined in this manner are shown in Figures 4 and 5. To illustrate the span of actual frequencies

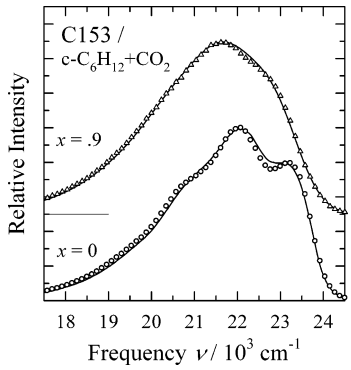

Figure 3. Examples of the fits (solid curves) to spectral data (points) described in the text. Spectra are emission spectra from the c-C_6H_{12} system at the compositions indicated.

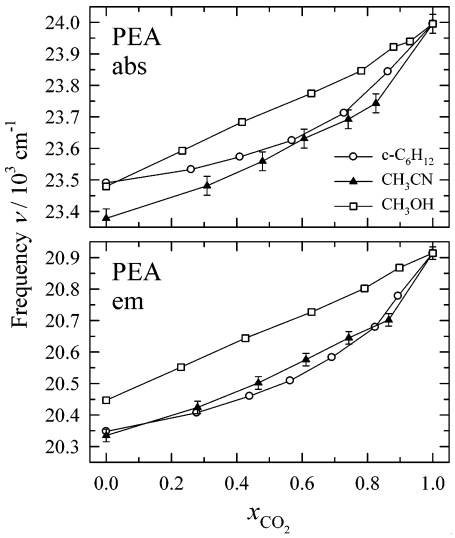

Figure 4. Absorption and emission frequencies of PEA in the three CO_2-expanded liquid systems. The frequencies plotted here are approximate first moment frequencies calculated by adding the first moment frequencies in the 2-methylbutane reference solvent (ν_{abs} = 23 630 cm^{-1}, ν_{em} = 20 550 cm^{-1}) to the fitted shifts. The error bars included with the $CH_3CN + CO_2$ data are representative.

covered by the spectra, to the fitted shifts we have added back the first moment frequencies of the 2MB reference spectra. With the exception of the emission spectra of C153 in c-C_6H_{12} + CO_2, all spectra shift to the blue with increasing CO_2 concentration. This movement toward the gas-phase frequencies indicates a weakening of the differential (S_1-S_0) solute−solvent interactions as CO_2 is added. As will be seen from the simulations, the exceptional case of C153 emission in c-C_6H_{12} + CO_2 results from fact that the increase in electrostatic interactions available with CO_2 relative to the nonpolar solvent c-C_6H_{12} overcomes the decrease in the strength of nonpolar interactions as x_{CO_2} is increased, producing a net red shift. The observed frequencies shown in Figures 4 and 5 are generally nonlinear functions of composition. They range from being very nearly linear in the case of PEA in $CH_3OH + CO_2$ to being markedly nonlinear for C153 in the CH_3CN and CH_3OH mixtures. As will be discussed shortly, such nonlinearity might be interpreted in terms of preferential solvation.

Before doing so we first consider the differences observed between the absorption and the emission shifts. In the case of PEA, the solvent dependence of the frequencies in absorption and emission is identical to within experimental uncertainties. Such behavior would be expected based on the liquid-phase results in Figure 1. The absorption and emission shifts of C153,

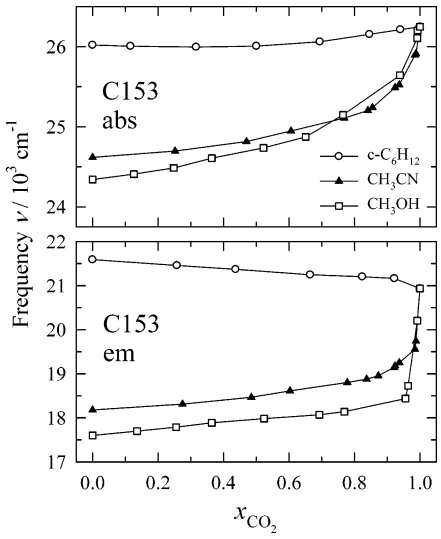

Figure 5. Absorption and emission frequencies of C153 in the three CO_2-expanded liquid systems. The frequencies plotted here are first moment frequencies calculated by adding the first moment frequencies in the 2-methylbutane reference solvent (ν_{abs} = 26 280 cm^{-1}, ν_{em} = 21 470 cm^{-1}) to the fitted shifts. Uncertainties are approximately the size of the symbols.

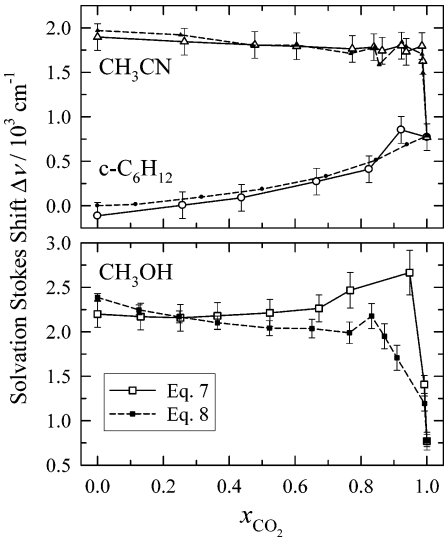

Figure 6. Solvent-induced Stokes shifts of C153 calculated using eq 7 (open symbols and solid curves) and eq 8 (small filled symbols and dashed curves).

however, are significantly different in all three solvents. Estimates of the solvent contribution to the Stokes shifts (or twice the solvent reorganization energies) of C153 are summarized in Figure 6. The open symbols here are calculated directly from differences between the absorption and the emission shifts relative to the 2MB reference

$$\Delta\Delta\nu_{solv} = (\nu - \nu_{2MB})_{abs} - (\nu - \nu_{2MB})_{em} \qquad (7)$$

As noted in previous work,[69,72−74] the underlying vibronic structure in the emission of C153 depends on solvent polarity, and this dependence leads to additional uncertainty (±100 cm^{-1}) in separating solvent from intramolecular contributions to the Stokes shift. As an independent measure of $\Delta\nu_{solv}$ we therefore also use linear response estimates based on the observed broadening of the absorption spectrum

$$\Delta\nu_{solv} = f\frac{\sigma_{inh}^2}{k_B T} \tag{8}$$

In this expression σ_{inh} is the standard deviation of the Gaussian broadening function required to fit the absorption spectrum, k_B is Boltzmann's constant, and T is the temperature. Ideally, the factor f should be unity, but measurements in a wide range of solvents indicate that $f = 0.8$ for C153.[73] We therefore used $f = 0.8$ to produce the small filled symbols in Figure 6. There is good agreement between the values of $\Delta\nu_{solv}$ calculated according to eqs 7 and 8 in the cases of c-C_6H_{12} + CO_2 and CH_3CN + CO_2. In the c-C_6H_{12} + CO_2 mixture, $\Delta\nu_{solv}$ increases monotonically from zero as the CO_2 concentration increases. In CH_3CN + CO_2 the Stokes shift decreases by a surprisingly small amount, less than 10%, from the limit of pure CH_3CN ($\sim$2000 cm^{-1}) up to $x_{CO_2} = 0.9$, before it drops precipitously to its value in neat CO_2 ($\sim$750 cm^{-1}). The behavior in the CH_3OH + CO_2 mixture (bottom panel of Figure 7) is less clear. The two methods of calculating $\Delta\nu_{solv}$ disagree at intermediate CO_2 concentrations. In particular, the values of $\Delta\nu_{solv}$ calculated using eq 7 increase significantly with increasing x_{CO_2} between $x_{CO_2} = 0.4-0.9$, whereas those calculated using eq 8 decrease. This discrepancy presumably reflects complications due to changes in the underlying emission line shape with composition. Without further study we take as the best estimate of $\Delta\nu_{solv}$ the average of the values obtained from these two methods. From this perspective, the solvation Stokes shifts in CH_3OH + CO_2 are seen to be similar to those in CH_3CN + CO_2 in that they change little over a wide composition range and only decrease relatively abruptly to the neat CO_2 value beyond $x_{CO_2} = 0.9$.

The final and most important aspect of the experimental data concerns what the spectral shifts suggest about the local solvent composition in the vicinity of these solutes. As mentioned in the Introduction, the usual assumption is that, in the absence of preferential solvation, a linear relationship should hold between frequency and composition[14]

$$\nu = x(1)\nu_1 + x(2)\nu_2 \tag{9}$$

where ν_1 and ν_2 are the frequencies observed in the pure component solvents and the $x(i)$'s are their mole fractions in the mixture. Under this assumption, the local composition of component 1 in the cybotactic region can be determined from

$$x_u^{\nu}(1) = \frac{\nu_{obs} - \nu_2}{\nu_1 - \nu_2} \tag{10}$$

(Here and in the following discussion we use (i) to denote component i and the subscript "u" to indicate compositions in the vicinity of the solute.) The local compositions calculated in this manner are only apparent compositions both because they rely on the validity of eq 9 and because the region to which they refer depends upon the observable measured ("ν" here). It is commonly assumed that electronic spectra are sensitive to the first solvation shell of the solute. As will be discussed, the simulations indicate that this assumption is correct.

Figure 7 illustrates the apparent local compositions so determined using the emission frequencies of PEA and C153. Absorption data yield similar results in the case of PEA whereas in C153 they tend to give smaller values of $x_u^{\nu}(1)$. Rather than plotting $x_u^{\nu}(1)$ directly, we instead plot apparent "enrichment factors", $x_u^{\nu}(1)/x(1)$, the ratios of the local mole fraction of component 1 (the liquid component) in the vicinity of the solute compared to its bulk value. In the case of PEA, the apparent enrichment amounts to relatively modest factors of 2−3 at the highest CO_2 concentrations studied. In C153, the much greater nonlinearities exhibited by the data in Figure 5, especially in emission, produce much larger apparent enhancement factors. Factors of $x_u^{\nu}(1)/x(1) > 30$ are obtained from eq 10 in the case of the CH_3CN + CO_2 and CH_3OH + CO_2 systems at $x_{CO_2} \geq 0.95$. It seems unlikely that the extent of preferential solvation could be as large as indicated by these numbers. The simulation results described in section 6 confirm this suspicion.

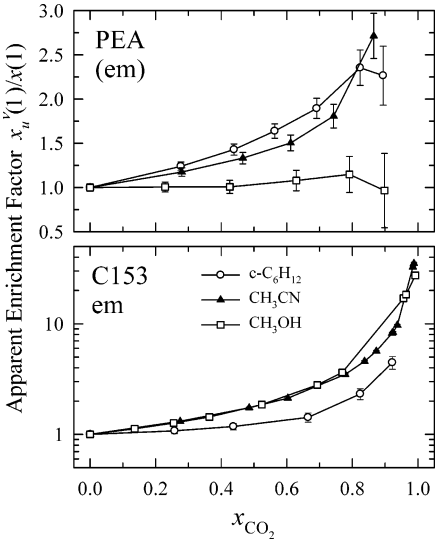

Figure 7. Apparent enrichment factors $x_u^{\nu}(1)/x(1)$ calculated from observed emission frequencies according to eq 10.

5. Experiment−Simulation Comparisons

The spectroscopic model adopted here assumes that the spectral shifts of a given solute in any solvent can be represented by a sum of electrostatic and dispersion contributions of the form

$$h(\nu - \nu_{gas})_{abs} = f\langle U_{dsp}\rangle_0 + \langle \Delta U_{el}\rangle_0 \tag{11a}$$

$$h(\nu - \nu_{gas})_{em} = f\langle U_{dsp}\rangle_1 + \langle \Delta U_{el}\rangle_1 \tag{11b}$$

where $\langle x\rangle_i$ indicates averaging over a simulated trajectory in the presence of the solute with charges appropriate to state i = 0 or 1 (S_0 or S_1). The quantities needed for calculating U_{dsp} (eqs 3 and 4) and ΔU_{el} (eq 5) are determined from solute and solvent parameters taken from standard force fields and solute charges derived from electronic structure calculations. For each solute a single parameter, f, the fractional increase in dispersion interactions between the S_0 and the S_1 states, is used as an adjustable parameter with which to fit the experimentally observed frequencies. Optimizing the value of f to best fit the gas-to-solution shifts observed in the neat solvents CO_2, c-C_6H_{12}, CH_3CN, and CH_3OH yielded values of $f = 0.15$ and $f = 0.21$ for PEA and C153, respectively. Such values, which indicate increases of 15−20% in dispersion interactions upon electronic excitation, seem reasonable.

The ability of this model to fit the experimental data is illustrated in Figure 8. (Simulated shifts and other quantities are tabulated in the Tables S5−7 in the Supporting Information.) The left-hand panels of Figure 8 show comparisons for the PEA/anthracene solute. Recall that for comparison to PEA experiments we use simulations of anthracene, the chromophore of PEA.[75] Additionally, because of the negligible differences observed between the absorption and the emission

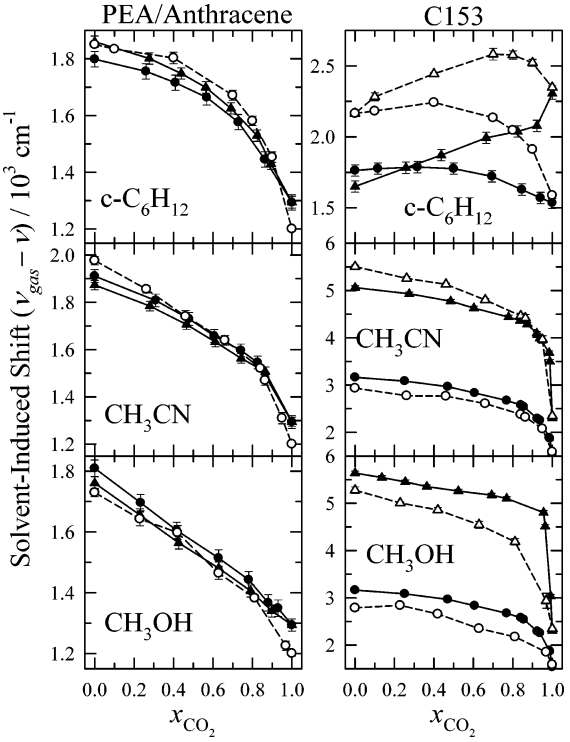

Figure 8. Observed (filled symbols and solid lines) and simulated (open symbols and dashed lines) solvent-induced shifts in the absorption (circles) and emission (triangles) frequencies of PEA (anthracene simulations) and C153. The experimental shifts were calculated from shifts measured relative to 2-methylbutane assuming references shifts ($\nu_{gas} - \nu_{2MB}$) of 1660 cm^{-1} in PEA and 1500 cm^{-1} in C153 for both absorption and emission.

shifts of PEA we have simulated only absorption shifts here. Despite these shortcuts, Figure 8 shows that there is generally good agreement between the simulated and the experimental shifts of PEA/anthracene. In agreement with the solvatochromic analysis associated with Figure 1, the charge differences computed via AM1/CI calculations for anthracene (and PEA) are small and lead to almost negligible contributions of ΔU_{el} to the calculated shifts. For this reason, and because the dispersion interactions are not greatly different in the three liquid solvents, the simulated shifts, like the experimental shifts, are comparable in all three GXLs. Also like experiment, the nonlinearity in the simulated composition dependence is smaller in the $CH_3OH + CO_2$ system compared to those of the other two mixtures.

In the case of the C153 solute (right-hand panels of Figure 8) there is a greater variety of behavior of the simulated and observed shifts. As will be discussed more below, electrostatic and dispersion interactions make comparable contributions to the net shifts in almost all cases. The poorest agreement between simulated and experimental shifts is found in the c-$C_6H_{12} + CO_2$ system, where it appears that the dispersion interactions between C153 and c-C_6H_{12} are overestimated by approximately 25%, perhaps as a result of using a united atom model for c-C_6H_{12}. Nevertheless, the simulations are able to reproduce the unusual net blue shift of the absorption and red shift of the emission with increasing CO_2 concentration that is observed in experiment. As mentioned previously, the interpretation offered by simulation is that these contrary trends result from the smaller dispersion but larger electrostatic interactions between C153 and CO_2 compared to c-C_6H_{12} combined with the different proportions of these two interactions in the absorption versus emission shifts. In the case of the $CH_3CN + CO_2$ system the simulations do an excellent job of reproducing experiment. C153 in $CH_3OH + CO_2$ represents an intermediate case, in which the absorption shifts are reasonably reproduced, apart from an overall displacement, but the emission shifts show a much more gradual decrease with x_{CO_2} than is found experimentally. We also note that the solvent contributions to the Stokes shifts (Figure S1) are also reasonably reproduced in all three GXLs, especially if one uses the experimental estimates calculated via eq 8.

On the basis of the above observations, we conclude that the simulation and spectroscopic models employed here provide physically reasonable and semiquantitative representations of the electronic spectral shifts of both PEA and C153 in the three GXLs studied. It is therefore appropriate to use these simulations to explore the general relationships between spectral shifts and local environment in such systems. In particular, we seek to understand to what extent analyses of spectral shifts like that leading to Figure 7 provide accurate measures of preferential solvation in GXLs.

6. Local Environment and Spectral Shifts

We examine solvation structure and preferential solvation here by considering mainly local compositions averaged over the first solvation shell of the solute. For this purpose we use "solvation shell distribution functions",[59] which provide information similar to what is provided by conventional radial distribution functions in atomic systems. The solvation shell distribution function $g_{ss}(r)$ is defined as the relative probability of finding a solvent atom of a particular type at a distance r from the closest solute atom, normalized such that $g_{ss}(r) = 1$ for a random distribution of solvent molecules. Representative $g_{ss}(r)$ functions of the C153 solute are shown in Figure 9, where we have plotted distributions of atoms of the CO_2 and liquid-component molecules undifferentiated with respect to atom type. Corresponding distributions for the anthracene solute are similar but reflect somewhat less preferential solvation. The green and red curves in Figure 9 denote distributions about C153(S_0) at the lowest and highest CO_2 concentrations, respectively. Data at the remaining compositions fall approximately between these limits. Distributions for C153 in the S_1 state at the highest values of x_{CO_2} are also provided as the blue curves in the right-hand panels.

Most of the $g_{ss}(r)$ functions shown in Figure 9 exhibit a prominent first peak and the oscillations typical of dense liquid packing. In the pure solvents, peak values of $g_{ss}(r)$ fall in the range 1.75−2.5, and similar values are found in all of the mixed solvents except at the highest CO_2 concentrations. As illustrated here, the distributions of CO_2 atoms are fairly similar in all three mixtures. In the CO_2 $g_{ss}(r)$ functions we observe oscillatory structure that often extends to 2−3 solvation shells. Interestingly, this structure is more pronounced in the mixtures more dilute in CO_2. The distributions of the liquid-component atoms show more variable behavior. The $g_{ss}(r)$ functions of CH_3CN atoms in $CH_3CN + CO_2$ mixtures are most similar in appearance to those of CO_2, an unsurprising result given the similar geometries of these two molecules. In the case of c-C_6H_{12}, neat or in c-$C_6H_{12} + CO_2$ mixtures, shoulders are observed on the main peak of $g_{ss}(r)$ due to the multiple atom−atom distances present within c-C_6H_{12}. Finally, in the case of C153 interacting with CH_3OH, the first solvation shell peak at high x_{CO_2} is split into several peaks, one at ∼2 Å and two near 3 Å, as a result of solute−solvent hydrogen bonding. Examination of atom−atom distribution functions shows that the carbonyl oxygen of C153 frequently accepts a hydrogen bond from CH_3OH. Using a simple distance criterion, $r_{OH} < 2.6$ Å, we estimate that in the S_0 state C153 is hydrogen-bonded approximately 75%

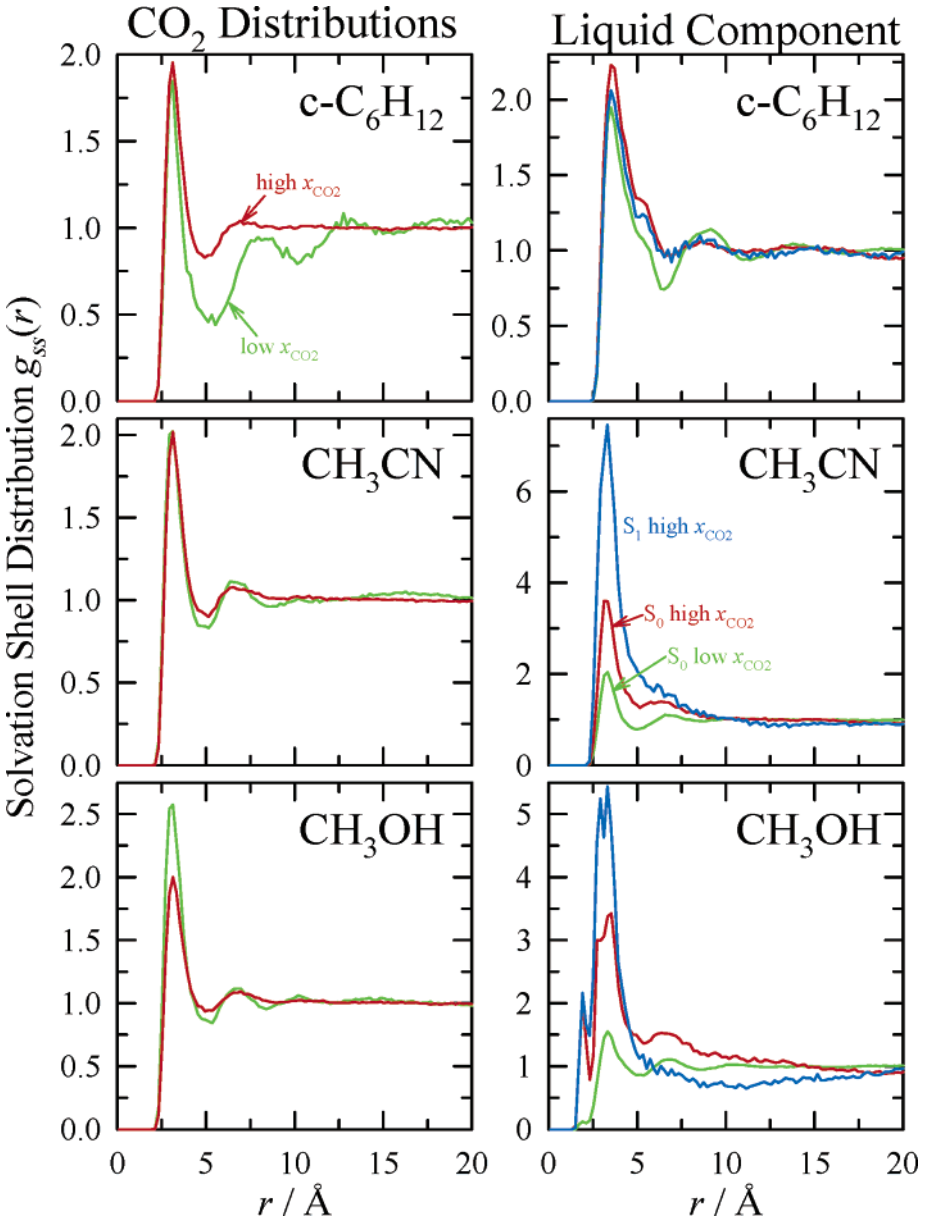

Figure 9. Solvation shell distribution functions $g_{ss}(r)$ observed around the C153 solute. The left-hand panels are the distributions of CO_2 atoms, and the right-hand panels the distributions of atoms of the liquid component. Green and red curves denote distributions about the C153(S_0) solute at the lowest and highest values of x_{CO_2} simulated (0.1 and 0.9 in c-C_6H_{12}, 0.262 and 0.95 in CH_3CN, and 0.23 and 0.97 in CH_3OH). Blue curves show the corresponding distributions about C153 in the S_1 state. (Only liquid-component and highest CO_2 concentration data are shown for the S_1 state, because they differ most from the S_0 distributions.)

of the time in neat CH_3OH and approximately ~35% of the time at the highest CO_2 concentration studied, $x_{CO_2} = 0.97$. In the S_1 state the fractions are 30−40% larger. We do not analyze these hydrogen-bonding interactions further. As will be described presently, quite similar behavior is found for C153 in the c-C_6H_{12} + CO_2 and CH_3CN + CO_2 mixtures where no such specific interactions occur. This similarity indicates that specific interactions are of secondary importance to the phenomena of interest here.

One final aspect of the liquid-component distributions that should be noted from Figure 9 relates to a shortcoming of the present simulations. At the highest CO_2 concentrations simulated, $g_{ss}(r)$ sometimes differs slightly from unity at large r. The departure is most clearly displayed by the C153 in CH_3OH + CO_2 data at large x_{CO_2} but is also found for C153 in CH_3CN + CO_2 and to a lesser extent in other systems. If one assumes that significant spatial correlations do not extend beyond 20 Å (nearly half of the simulation box lengths used here), then this departure can be due to either incomplete averaging of $g_{ss}(r)$ or to insufficient numbers of the liquid-component molecules to establish the expected bulk mole fractions at large r. In the most extreme cases, C153(S_1) in CH_3CN + CO_2 and C153(S_1) in CH_3OH + CO_2 at the highest x_{CO_2} concentrations (blue curves in Figure 9), it appears that the extensive aggregation around the solute depletes the supply of liquid-component molecules (only 50 and 31, respectively) such that the bulk ($r \rightarrow 20$ Å) mole fractions are only 90% of their expected values. In these particular systems, the simulations therefore depart slightly from the targeted experimental conditions. We anticipate that this departure is roughly equivalent to an uncertainty in the proper bulk compositions of these systems. For example, instead of the experimental values of x_{CO_2}, we have $0.95 \leq x_{CO_2} \leq 0.96$ in the CH_3CN + CO_2 simulation and $0.97 \leq x_{CO_2} \leq 0.98$ in the CH_3OH + CO_2 simulation. Uncertainties of this magnitude should not significantly influence interpretation of the simulations.

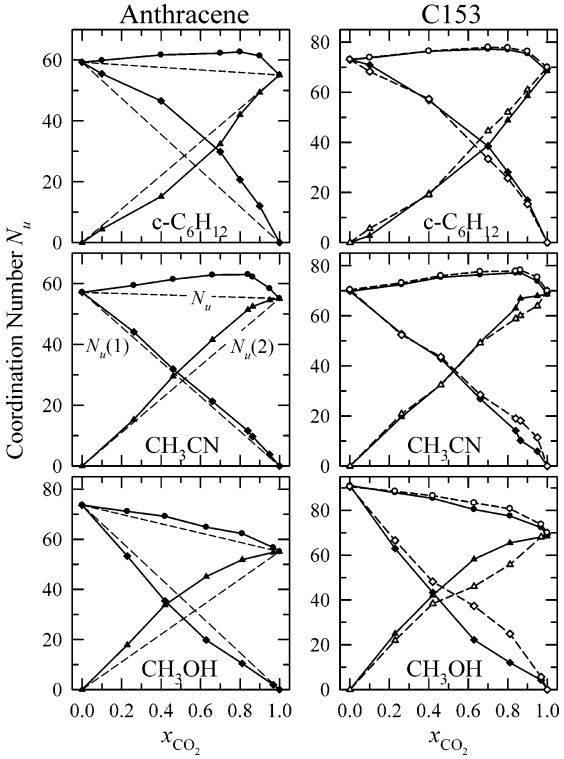

Figure 10. First solvation shell coordination numbers of anthracene (left-hand panels) and C153 (right-hand panels). Diamonds, triangles, and circles represent numbers of atoms of the liquid component $N_u(1)$, numbers of CO_2 atoms $N_u(2)$, and their sum N_u, within 5 Å of any solute atom. In the case of C153 the filled symbols and solid lines are distributions in the presence of the S_0 charges whereas the open symbols and dashed lines are those of the S_1 solute. (The dashed lines in the left-hand panels simply connect the $x = 0$ or 1 extremes.) Uncertainties in these values are approximately the size of the symbols.

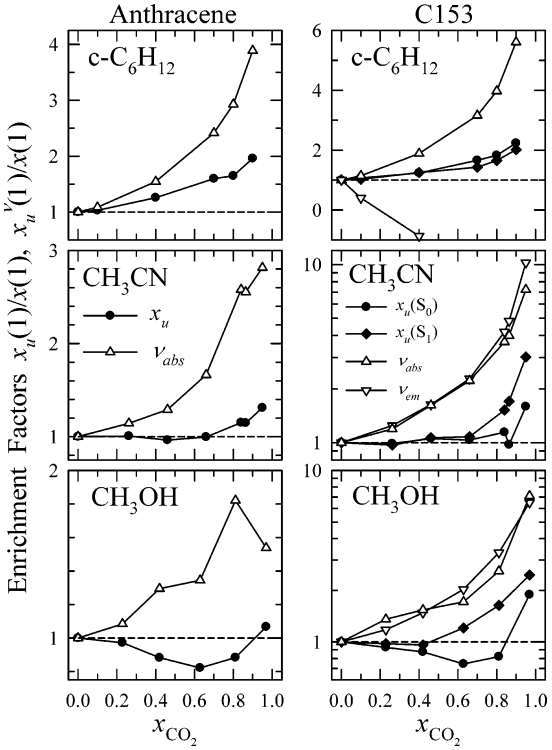

Figure 11. Simulated enrichment factors $x_u(1)/x(1)$ (filled symbols) in the first solvation shells of anthracene and C153 (eq 12) and apparent enrichment factors $x_u^{\nu}(1)/x(1)$ determined using the simulated absorption and emission frequencies according to eq 10 (open symbols).

Having discussed some details of the spatial solvation structure, we now focus exclusively on the immediate neighborhood of the solute. Coordination numbers, defined as the number of atoms within 5.0 Å of the solute, obtained by integrating $g_{ss}(r)$ distributions, are shown in Figure 10. (See also Tables S5−7.) Shown in Figure 10 are the numbers of atoms of the liquid component, $N_u(1)$, of CO_2, $N_u(2)$, and the total numbers of atoms belonging to any solvent molecule, N_u. In the left-hand panels (anthracene data) the dashed lines indicate "ideal" mixing behavior.

One important feature displayed in Figure 10 is the fact that all of the total coordination numbers N_u exhibit positive deviations from ideality shown by the total coordination numbers. The effect is most pronounced in the $CH_3CN + CO_2$ system and least apparent in $CH_3OH + CO_2$, but it is present in all of the solute/solvent combinations studied. This relative densification in the first coordination shell is presumably related to the fact that the mass density of these GXLs goes through a maximum in the vicinity of $x_{CO_2} = 0.7-0.8$ (see Figure 1 of ref 36). Such an interpretation is supported by the fact that for all three mixtures the departures from ideality are quite similar in anthracene, C153(S_0), and C153(S_1). As will be discussed later, this effect has important consequences for the interpretation of solvatochromic shifts in GXLs. Another feature shown in Figure 10 is the fact that the individual component coordination numbers of liquid and CO_2 atoms often deviate in opposite ways from ideality. For example, in the anthracene/c-$C_6H_{12} + CO_2$ system there is a deficit of CO_2 atoms at the same time there is an excess of c-C_6H_{12} atoms, indicating that anthracene is preferentially solvated by c-C_6H_{12}.

The extent of preferential solvation is better displayed in Figure 11 where we plot "enrichment factors" (filled symbols)

$$\frac{x_u(1)}{x(1)} = \frac{N_u(1)/N_u}{x(1)} \tag{12}$$

where $x_u(1)$ is the mole fraction of component 1, the liquid component, in the first coordination shell of the solute and $x(1)$ is its bulk mole fraction. In most cases, and in all systems at sufficiently high CO_2 concentrations, the first solvation shells of anthracene and C153 are enriched in the liquid component. Maximal enrichments in the range of 2−3 are observed for $x_{CO_2} > 0.9$. However, in $CH_3OH + CO_2$ mixtures the less polar solutes anthracene and C153(S_0) are preferentially solvated by CO_2 at intermediate compositions. Such variations in the extent of preferential solvation with solute, GXL, and composition reflect a complex interplay between solute−solvent interactions and solvent−solvent interactions.[14] We do not attempt to dissect these variations further. We merely observe that differences in (largely) nonpolar interactions such as exist in anthracene in c-$C_6H_{12} + CO_2$ and in C153 in c-$C_6H_{12} + CO_2$ are sufficient to give rise to 2-fold preferences in these model solutions. Not surprisingly, the systems with the most polar solute−solvent interactions, C153(S_1) in the CH_3CN and CH_3OH mixtures, show the greatest preferential solvation. The values of $x_u(1)/x(1)$ observed here are comparable to the corresponding quantities measuring the preference for solvation of the liquid component by other liquid molecules in the absence of a solute we previously reported in these mixtures.[36]

What is of primary interest to the present work is the fact that the preferential solvation in these mixtures is in all cases grossly misrepresented by inserting the simulated frequencies into eq 10. The latter estimates are shown as the open symbols in Figure 11. These simulated values of $x_u^{\nu}(1)/x(1)$ agree

semiquantitatively with the estimates based on experimental emission frequencies in Figure 7. There is comparable agreement for the absorption frequencies not shown in Figure 7, except in the case of C153 in c-C_6H_{12} + CO_2. In this latter system, the small magnitude of the shifts together with the errors in the simulated values (Figure 8) produce large negative values of $x_u^v(1)/x(1)$ at higher x_{CO_2}'s. This latter behavior is a clear indication of the breakdown of the assumptions underlying eq 10, as is the dramatic departure of these apparent enhancement factors from the true values of $x_u(1)/x(1)$ that they are meant to represent. We now analyze the reasons for this departure.

As modeled here, frequency shifts are composed of additive contributions from two distinct types of interactions, electrostatic and nonpolar. Because these two contributions differ in their composition dependence, it is best to consider them separately. For added perspective, we discuss not only the energy differences ΔU_{el} and ΔU_{dsp} relevant for the frequency shifts (eqs 1−5) but also the electrostatic interaction energies U_{el} and Lennard-Jones interaction energies U_{LJ} between the solvent and the solute in its two electronic states. Data on all of these components are provided in Tables S5−7 of the Supporting Information.

In keeping with the dominance of nonpolar interactions in PEA (Figure 1) or anthracene[46] the simulated spectral shifts of anthracene are completely dominated (>99%) by ΔU_{dsp}. The simulated solute−solvent interaction energies are also primarily (>85%) due to nonpolar interactions, U_{LJ} (Figure S2 of the Supporting Information). We will not describe the composition dependence of the anthracene energies further because they behave similarly to the nonpolar components of the energies, ΔU_{dsp} and U_{LJ}, observed in C153. In contrast to anthracene, electrostatic contributions to the interaction energies are comparable in magnitude to the nonpolar contributions in the C153 solute (Figure S3). In the polar mixtures CH_3CN + CO_2 and CH_3OH + CO_2, electrostatic energy differences ΔU_{el} account for ∼60% of the emission shifts and ∼30% of the absorption shifts (and they account for essentially all of the Stokes shift). Even in pure CO_2, the present simulations indicate that electrical contributions are ∼40% in emission but only ∼10% in absorption.

Figure 12 shows the apparent enrichment factors x_u^A/x reported by different energy quantities A of the C153 (S_1) solute using a relation analogous to eq 10,

$$x_u^A(1) \equiv \frac{\langle A\rangle_{obs} - \langle A\rangle_2}{\langle A\rangle_1 - \langle A\rangle_2} \qquad (13)$$

where brackets indicate a simulation average and the subscripts 1 and 2 denote values in the pure component solvents. For comparison, the actual enrichment factors determined from coordination numbers via eq 12 are shown by the filled symbols in Figure 12. As with the enrichment factors based on spectral shifts in Figure 11, the apparent enrichment factors determined from individual energy components differ markedly from the correct values. In most cases, local compositions determined from eq 13 indicate a greater preferential solvation by the liquid component than is actually present, with the exception being when electrical interactions are considered in the c-C_6H_{12} + CO_2 system. An important feature displayed in Figure 12 is the fact that the values of x_u^A determined from ΔU_{el} and U_{el} are nearly equal in most cases, as are those determined from ΔU_{dsp} and U_{LJ}. Thus, the electrostatic versus nonpolar character of the interactions seems to be more important than the details of the charge distribution involved (Δq_α vs q_α) or whether repulsive interactions (present in U_{LJ} but not ΔU_{dsp}) are included or not.

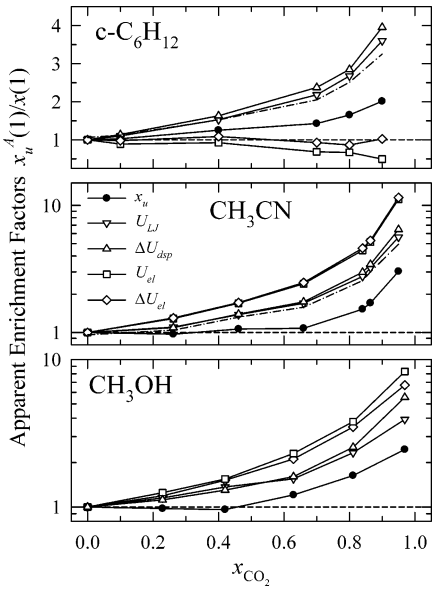

Figure 12. Apparent enrichment factors ($x_u^A(1)/x(1)$, open symbols) calculated from various energy quantities according to eq 13 for the solute C153(S_1). Quantities considered are the Lennard-Jones (U_{LJ}) and electrostatic (U_{el}) components of the solute−solvent interaction energies and the S_1-S_0 differences in dispersion (ΔU_{dsp}) and electrostatic (ΔU_{el}) interaction energies from which the spectral shifts are calculated. Also shown for reference are the true enrichment factors $x_u(1)/x(1)$ (filled symbols). The dot−dashed lines in the top two panels denote values calculated according to eq 16 when $A = U_{LJ}$.

TABLE 1: First Solvation Shell Energy Fractions[a]

solute	solvent	$f_1(U_{LJ})$	$f_1(\Delta U_{dsp})$	$f_1(U_{el})$	$f_1(\Delta U_{el})$
anthracene	c-C_6H_{12} + CO_2	0.85	0.90	0.99	
	CH_3CN + CO_2	0.83	0.90	0.99	
	CH_3OH + CO_2	0.82	0.89	0.96	
C153(S_0)	c-C_6H_{12} + CO_2	0.86	0.91	0.96	0.83
	CH_3CN + CO_2	0.85	0.91	0.94	0.79
	CH_3OH + CO_2	0.84	0.91	0.93	0.73
C153(S_1)	c-C_6H_{12} + CO_2	0.86	0.91	0.93	0.90
	CH_3CN + CO_2	0.85	0.91	0.90	0.89
	CH_3OH + CO_2	0.84	0.91	0.88	0.85

[a] Values listed are the fractions of the energy of a given type contributed by solvent molecules having at least one atom within 5 Å of the solute, averaged over all compositions of a given mixture. The values of ΔU_{el} are not reported for anthracene because these energy differences are too small in the present model to measure reliably.

In addition, the values of x_u^A determined from nonpolar interactions can sometimes be quite different (in c-C_6H_{12} + CO_2, for example) than those determined from polar electrostatic interactions.

What are the reasons for these differences and for the inaccuracy of eq 13 for measuring local compositions? It would be reasonable to suppose that the different ranges of electrostatic versus nonpolar interactions might be important and that perhaps these energies are not measuring solely first solvation shell properties. However, in all of the systems simulated, we find that 80% or more of these solute−solvent interaction energies are determined by molecules within the first solvation shell of the solute. This fact is documented in Table 1, where we list fractions f_1 of the various energy components contributed by molecules having at least one atom within the first solvation shell of the solute. For brevity, the values listed here have been averaged over all compositions of a given system, but variations with composition are not large. Overall, the fractions are ordered $f_1(\Delta U_{el}) < f_1(U_{LJ}) < f_1(\Delta U_{dsp}) < f_1(U_{el})$ with average values of 83%, 85%, 91%, and 94%. Thus, these energy components,

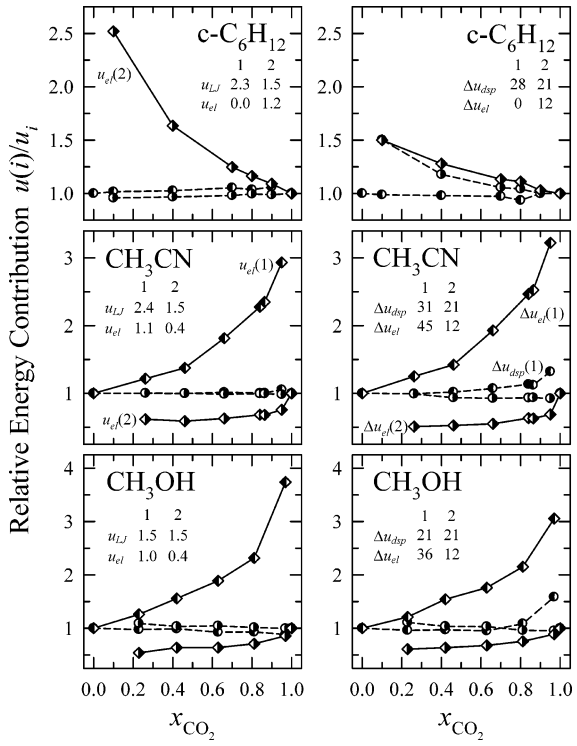

Figure 13. Relative per-atom contributions (eq 14) from the two solvent components to various energy quantities of C153(S_1). The left-hand panels contain the Lennard-Jones (u_{LJ}, circles) and electrical (u_{el}, diamonds) components of the solute−solvent interaction energy. The right-hand panels contain the S_1-S_0 differences in dispersion (Δu_{dsp}, circles) and electrical (Δu_{el}, diamonds) interaction energies from which spectral shifts are calculated. Left-filled symbols denote contributions from component 1 (the liquid component), and right-filled symbols contributions from component 2 (CO_2). All data are normalized to the values in the pure solvent components. The inset tables provide the normalizing values in units of kJ/mol (left panels) and cm^{-1} (right panels).

which combine to form the solvation energies and spectroscopic observables, are largely short-range quantities that report on conditions within the first solvation shell. Moreover, because x_u measures the composition near the maximum in $g_{ss}(r)$, the presence of contributions from regions at larger distances would only tend to reduce apparent enrichment factors and cannot explain the fact that values of $x_u^A(1)$ tend to be larger than the values of $x_u(1)$.

The differences observed in Figure 12 can instead be traced to two other effects. The first is related to the collective character of electrostatic interactions. This effect is explored in Figure 13, where we plot relative contributions to the various energies of C153(S_1) on a per-atom basis

$$a(i) \equiv \frac{\langle A(i)\rangle}{\langle N_u(i)\rangle} \tag{14}$$

where $\langle A(i)\rangle$ represents the average contribution of solvent molecules of type $i = 1$ or 2 to the energy quantity A. For example, $u_{LJ}(1)$ is the simulation-averaged contribution of molecules of the liquid component (1) to the Lennard-Jones solute−solvent interaction energy, U_{LJ}, normalized by the average number of liquid-component atoms in the first solvation shell. When considered relative to the same values in the pure liquid state of component i (denoted a_i) as in Figure 13, we expect these quantities to accurately reflect the per-molecule contributions to the various energies contributed by first solvation shell molecules. As illustrated in Figure 13, a clear distinction exists between the nonpolar and electrostatic components of the energies. The nonpolar per-atom energies u_{LJ} and Δu_{dsp} are nearly independent of mixture composition whereas the electrostatic energies u_{el} and Δu_{el} are decidedly not.

The Lennard-Jones contributions to the solvation energies are especially insensitive to composition. We observe at most a few percent variation in the values of $u_{LJ}(i)$ in all of the systems studied. Similarly accurate scaling with coordination number has been noted previously in the context of density augmentation in supercritical fluids.[76,77] Lennard-Jones energies are therefore nearly ideal reporters of coordination numbers in the sense that

$$\langle A\rangle = \langle N_u(1)\rangle a_1 + \langle N_u(2)\rangle a_2 \tag{15}$$

for $A = U_{LJ}$. On this basis, one might expect Lennard-Jones energies to provide accurate measures of local composition, and they would if not for the second factor discussed below. The situation is slightly less favorable with respect to the dispersion interactions. Values of Δu_{dsp} vary by up to 50% with composition in some cases. But dispersion energies, like Lennard-Jones energies, can, in most of the cases studied, also be considered to be approximately additive in the number of atoms in the first solvation shell.

Additivity in the sense of eq 15 is clearly not true of electrostatic interactions. As shown in Figure 13, electrostatic energies on a per-atom basis vary by factors of 3 or more for the liquid-component species and typically by a factor of approximately 2 for CO_2 + solute interactions. The fact that u_{el} and Δu_{el} always decrease with increasing polarity in a mixture reflects the fact that favorable electrostatic interactions between a solute and solvent molecules only come at some cost in unfavorable solvent + solvent interactions. The conflicting requirements of simultaneously optimizing both solute−solvent and solvent−solvent interactions renders quantities such as $\langle U_{el}\rangle$ inherently nonlinear in the number of polar solvent molecules in the first solvation shell. As a result, it is to be expected that the use of eq 13, which implicitly assumes additivity of the property A, will lead to incorrect results when electrostatic interactions play an important role, as they do in the spectral shifts of C153. Breakdown of the additivity assumption (eq 15) accounts for roughly half of the deviations between x_u and x_u^ν for C153 displayed in Figure 11.

The remaining discrepancies between x_u and x_u^ν come from a less obvious source, one which is special to gas-expanded liquids. It arises from the nonlinearity of the total coordination numbers as functions of composition noted in Figure 10. In all three of the GXLs studied, the experimentally observed maximum in mass density as a function of composition[36] leads to positive deviations in coordination numbers from what would be anticipated based on a linear interpolation between the neat solvent limits. This positive deviation usually renders the values of $x_u^A(1)$ calculated according to eq 13 larger than $x_u(1)$, even when the implicit assumption of additivity (eq 15) is accurate. To see why, assume some property A for which eq 15 holds exactly. For algebraic simplicity, further assume that the coordination numbers at the two neat solvent limits are equal, $\langle N_u\rangle_1 = \langle N_u\rangle_2 = N_u^\circ$, an approximation accurate to better than 5% for the solutes studied here in the c-C_6H_{12} + CO_2 and CH_3-CN + CO_2 mixtures. Under these assumptions one finds that x_u^A calculated using eq 13 is related to x_u via

$$x_u^A(1) = x_u(1)\left(1 + \frac{\Delta N_u}{N_u^\circ}\right) + \frac{\Delta N_u}{N_u^\circ}\left(\frac{a_2}{a_1 - a_2}\right) \tag{16}$$

where $\Delta N_u = \langle N_u \rangle - N_u^\circ$. Thus, for positive ΔN_u and $a_2/(a_1 - a_2)$, the situation prevailing here in the case of nonpolar interactions, $x_u^A(1) > x_u(1)$. Values of $\Delta N_u/N_u^\circ$ here are a mere 8%, but the increase of $x_u^A(1)$ relative to $x_u(1)$ is much larger due to the second term in eq 16. With the Lennard-Jones energies as an example, the x_u^A's calculated according to eq 16 are plotted as dot−dashed curves in the two top panels of Figure 12. As illustrated there, eq 16 provides a good approximation to the apparent enrichment factors calculated from the Lennard-Jones energies, demonstrating how a 2-fold exaggeration of the local compositions results from the much smaller departure of the coordination numbers from their interpolated values. This densification effect accounts for virtually all of the discrepancy between x_u^A and x_u in the case of LJ interactions and more than half of the discrepancy in the case of dispersive spectral shifts. Comparison of the x_u^A from Figure 12 and the relative energy contributions in Figure 13 indicates that this effect also accounts for approximately half of the difference between x_u^A and x_u in the case of electrostatic interactions.

To summarize the foregoing discussion, the present simulations indicate that attempts to measure local compositions in the vicinity of solutes in GXLs using simplistic approaches of the sort embodied in eqs 10 and 13 are not likely to provide accurate results. Simulated enrichment factors $x_u(1)/x(1)$ are not greater than 2−3 in the systems studied, whereas much larger factors are suggested by these equations when using either experimental or simulated spectral shifts. The inaccuracy of eq 13 stems from two sources. First, additivity of the sort described by eq 15 and implicit in eq 13 is a poor approximation in cases where electrostatic interactions are important. Second, even when eq 15 is satisfied, changes in coordination number will cause the composition dependence of solute energies to depart from the behavior anticipated in simple mixtures.

One can attempt to employ more sophisticated analyses to extract local compositions from spectral data. For example, the expected composition dependence of electrostatic interactions is often modeled using dielectric continuum descriptions of solvation.[78−80] In such descriptions the nonadditivity of electrostatic interactions (in the sense of eq 15) is accounted for in reaction field factors such as $f(\epsilon_r) = (\epsilon_r - 1)/(\epsilon_r + 2)$ via the nonlinear dependence of $f(\epsilon_r)$ on the relative permittivity ϵ_r and on composition. Figure 14 shows that the highly nonlinear composition dependence of the electrostatic quantities U_{el} and ΔU_{el} in the polar systems C153 in $CH_3CN + CO_2$ and C153 in $CH_3OH + CO_2$ is indeed largely accounted for, at least at lower x_{CO_2}'s, by using $f(\epsilon_r)$ for correlating these energies. Unfortunately, when CO_2 is the gaseous component, dielectric continuum models are not reliable over the entire composition range. Electrostatic interactions between a polar solute and the quadrupolar molecule CO_2 are not properly modeled using dielectric descriptions. As a result, at high CO_2 concentrations dielectric predictions are unreliable. The problem is evident in the data shown in Figure 14, where the simulated energies at the lowest values of $f(\epsilon_r)$ (highest x_{CO_2}) depart markedly from the linear correlations established at $x_{CO_2} < 0.8$. In neat CO_2 the simulated value of $f(\epsilon_r)$ is zero, meaning that no electrostatic interaction is predicted from a dielectric continuum model, whereas, in reality, electrostatic interactions in neat CO_2 are a sizable fraction of their magnitudes in polar solvents. For this reason, the composition dependence predicted by dielectric continuum models also cannot be used to determine local compositions in CO_2 + liquid solvent mixtures.

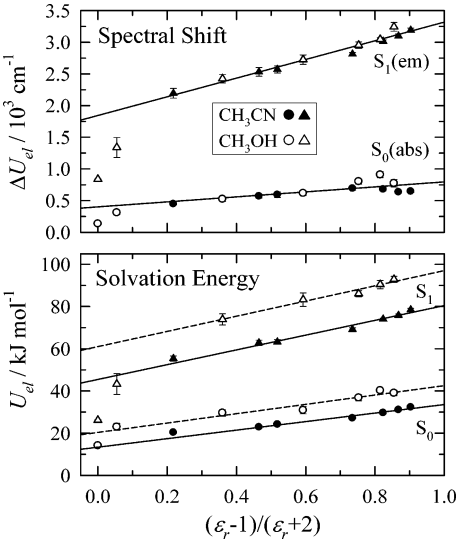

Figure 14. Correlation of the electrostatic component of the solute−solvent interaction energy U_{el} and the S_1-S_0 electrostatic energy difference ΔU_{el} of C153 with the relative permittivity ϵ_r of the two polar solvent mixtures $CH_3CN + CO_2$ and $CH_3OH + CO_2$. The lines shown here are least-squares fits to the data at compositions of $x_{CO_2} > 0.8$. In the case of ΔU_{el} a single correlation is observed with $f(\epsilon_r) = (\epsilon_r - 1)/(\epsilon_r + 2)$ in both solvent mixtures, as expected from dielectric continuum theories. In the case of U_{el} distinct correlations are found for the two solvent mixtures. Simulated permittivity data are from ref 36.

7. Summary and Conclusions

We have measured absorption and emission spectra of PEA and C153 in CO_2-expanded c-C_6H_{12}, CH_3CN, and CH_3OH. These systems were selected to include most of the types of solute−solvent interactions likely to be encountered in GXL systems. Apart from overall frequency shifts, no usual features were found in the spectra in expanded solvents compared to those in conventional liquid solvents. In nearly all cases the composition dependence of the frequency shifts suggests that these two solutes are preferentially solvated by the liquid-phase component of the mixture. Adopting the usual assumption that electronic frequency shifts report linearly on the composition in the cybotactic region, the extent of this preferential solvation appears to be quite large in many cases. For example, greater than 10-fold enrichment in CH_3CN and CH_3OH molecules in the cybotactic region of C153 is implied by such calculations at the highest CO_2 concentrations measured.

To better understand how to interpret the experimental shifts, we have also performed computer simulations of C153 and anthracene (the chromophore of PEA) in the three GXLs. These simulations employ a semiempirical model in which electronic spectral shifts are assumed to consist of additive contributions from electrostatic and dispersive interactions. Through the use of only a single adjustable parameter this model is able to provide reasonable representations of both the absorption and the emission shifts of C153 and PEA measured experimentally. The simulations show enrichment in the first solvation shell of these two solutes by the liquid components, qualitatively in accord with what was inferred from experiment. However, the extent of this enrichment is much smaller than that calculated based on a simplistic interpretation of the spectral shifts. The simulations show that the conventional assumption of a linear relationship between local composition and spectral shift is highly inaccurate in these systems. Two effects, the collective nature of electrostatic interactions and the fact that coordination numbers are not constant with composition, act together to

render such estimates of enrichment factors 2−5 times larger than the correct values. Dielectric modeling of the spectral shifts might help to correct these errors, but unfortunately, in the case of the quadrupolar molecule CO_2, dielectric estimates of solvation energies are inaccurate. These results lead to the rather pessimistic conclusion that simple interpretations of spectral shift data are unlikely to yield reliable determinations of local compositions in CO_2-expanded liquid mixtures.

Acknowledgment. This work was supported by funds from the National Science Foundation (Grant No. CHE-0241316) and the Petroleum Research Fund of the American Chemical Society. The authors thank Brian Laird and Kryzysztof Kuczera for helpful discussions and for preprints of their related studies.

Supporting Information Available: Geometry and force-field parameters of anthracene and C153, experimental frequency shifts of PEA and C153, simulated Stokes shifts of C153, fractions of the solute−solvent interaction energy of anthracene and C153 contributed by electrostatic interactions, and simulation results for anthracene and C153. This material is available free of charge via the Internet at http://pubs.acs.org.

References and Notes

(1) Eckert, C. A.; Bush, D.; Brown, J. S.; Liotta, C. L. *Ind. Eng. Chem. Res.* **2000**, *39*, 4615−4621.
(2) Eckert, C. A.; Liotta, C. L.; Bush, D.; Brown, J. S.; Hallett, J. P. *J. Phys. Chem. B* **2004**, *108*, 18108−18118.
(3) Hallett, J. P.; Kitchens, C. L.; Hernandez, R.; Liotta, C. L.; Eckert, C. A. *Acc. Chem. Res.* **2006**, *39*, 531−538.
(4) Besnard, M.; Tassaing, T.; Danten, Y.; Andanson, J.-M.; Soetens, J.-C.; Cansell, F.; Loppinet-Serani, A.; Reveron, H.; Aymonier, C. *J. Mol. Liq.* **2006**, *125*, 88−99.
(5) Anand, M.; McLeod, M. C.; Bell, P. W.; Roberts, C. B. *J. Phys. Chem. B* **2005**, *109*, 22852−22859.
(6) Dehghani, F.; Foster, N. R. *Curr. Opin. Solid State Mater. Sci.* **2003**, *7*, 363−369.
(7) Olesik, S. V. *J. Chromatogr., A* **2004**, *1037*, 405−410.
(8) Song, I.; Spuller, M.; Levitin, G.; Hess, D. W. *J. Electrochem. Soc.* **2006**, *153*, G314−G318.
(9) Wei, M.; Musie, G. T.; Busch, D. H.; Subramaniam, B. *Green Chem.* **2004**, *6*, 387−393.
(10) Lyon, C. J.; Sarsani, V. R.; Subramaniam, B. *Ind. Eng. Chem. Res.* **2004**, *43*, 4809−4814.
(11) Yeo, S.-D.; Kiran, E. *J. Supercrit. Fluids* **2005**, *34*, 287−308.
(12) de la Fuente Badilla, J. C.; Peters, C. J.; de Swaan Arons, J. *J. Supercrit. Fluids* **2000**, *17*, 13−23.
(13) Reichardt, C. *Solvents and Solvent Effects in Organic Chemistry*, 2nd ed.; VCH: Weinheim, Germany, 1988.
(14) Marcus, Y. *Solvent Mixtures: Properties and Selective Solvation*; Marcel-Dekker: New York, 2002.
(15) Kim, S.; Johnston, K. *AIChE J.* **1987**, *33*, 1603−1611.
(16) Kelley, S. P.; Lemert, R. M. *AIChE J.* **1996**, *42*, 2047−2056.
(17) Wyatt, V. T.; Bush, D.; Lu, J.; Hallett, J. P.; Liotta, C. L.; Eckert, C. A. *J. Supercrit. Fluids* **2005**, *36*, 16−22.
(18) Sala, S.; Tassaing, T.; Ventosa, N.; Danten, Y.; Besnard, M.; Veciana, J. *ChemPhysChem* **2004**, *5*, 243−245.
(19) Sala, S.; Ventosa, N.; Tassaing, T.; Cano, M.; Danten, Y.; Besnard, M.; Veciana, J. *ChemPhysChem* **2005**, *5*, 587−590.
(20) Yonker, C. R.; Smith, R. D. *J. Phys. Chem.* **1988**, *92*, 2374−2378.
(21) Ellington, J. B.; Park, K. M.; Brennecke, J. F. *Ind. Eng. Chem. Res.* **1994**, *33*, 965−974.
(22) Zhang, J.; Roek, D. P.; Chateauneuf, J. E.; Brennecke, J. F. *J. Am. Chem. Soc.* **1997**, *119*, 9980−9991.
(23) Bulgarevich, D. S.; Sako, T.; Sugeta, T.; Otake, K.; Sato, M.; Uesugi, M.; Kato, M. *J. Chem. Phys.* **1998**, *108*, 3915−3921.
(24) Chen, J.; Shen, D.; Wu, W.; Han, B.; Sun, D. *J. Chem. Phys.* **2005**, *122*, 204508.
(25) Kamlet, M. J.; Abboud, J. L. M.; Taft, W. R. *Prog. Phys. Org. Chem.* **1981**, *13*, 485−631.
(26) Reichardt, C. *Chem. Rev.* **1994**, *94*, 2319−2358.
(27) Pfund, D. M.; Fulton, J. L.; Smith, R. D. Aggregation of methanol in supercritical fluids: A molecular dynamics study. In *Supercritical Fluid Engineering Science: Fundamentals and Applications*; Kiran, E., Brennecke, J. F., Eds.; ACS Symposium Series 514; American Chemical Society: Washington DC, 1993; pp 158−174.
(28) Moon, S. D. *Bull. Korean Chem. Soc.* **2002**, *23*, 811−816.
(29) Chatzis, G.; Samios, J. *Chem. Phys. Lett.* **2003**, *374*, 187−193.
(30) Aida, T.; Inomata, H. *Mol. Simul.* **2004**, *30*, 407−412.
(31) Stubbs, J. M.; Siepmann, J. I. *J. Chem. Phys.* **2004**, *121*, 1525−1534.
(32) Houndonougbo, Y.; Guo, J.; Lushington, G. H.; Laird, B. *Mol. Phys.* **2006**, *104*, 2955−2960.
(33) Houndonougbo, Y.; Jin, H.; Rajagopalan, B.; Wong, K.; Kuczera, K.; Subramaniam, B.; Laird, B. *J. Phys. Chem. B* **2006**, *110*, 13195−13202.
(34) Houndonougbo, Y.; Laird, B.; Kuczera, K. *J. Chem. Phys.*, in press.
(35) Shukla, C. L.; Hallett, J. P.; Popov, A. V.; Hernandez, R.; Liotta, C. L.; Eckert, C. A. *J. Phys. Chem. B.* **2006**, *110*, 24101−24111.
(36) Li, H.; Maroncelli, M. *J. Phys. Chem. B* **2006**, *110*, 21189−21197.
(37) Skarmoutsos, I.; Samios, J. *J. Mol. Liq.* **2006**, *125*, 181−186.
(38) Cichos, F.; Brown, R.; Rempel, U.; von Borcyskowski, C. *J. Phys. Chem. A* **1999**, *103*, 2506−2512.
(39) Cichos, F.; Willert, A.; Rempel, U.; von Borczyskowski, C. *J. Phys. Chem. A* **1997**, *101*, 8179−8185.
(40) Patel, N. Simulations of Rotational Dynamics and Electronic Spectroscopy in Supercritical Fluids. Ph.D. Thesis, Pennsylvania State University, University Park, PA, 2003.
(41) Ando, K. *J. Chem. Phys.* **1997**, *107*, 4585−4596.
(42) Cichos, F.; Brown, R.; Bopp, P. A. *J. Chem. Phys.* **2001**, *114*, 6834−6842.
(43) Sulpizi, M.; Carloni, P.; Hutter, J.; Rothlisberger, U. *Phys. Chem. Chem. Phys.* **2003**, *5*, 4798−4805.
(44) Ingrosso, F.; Ladanyi, B. M.; Mennucci, B.; Elola, M. D.; Tomasi, J. *J. Phys. Chem. B* **2005**, *109*, 3553−3564.
(45) Ingrosso, F.; Tani, A.; Tomasi, J. *J. Mol. Liq.* **2005**, *117*, 85−92.
(46) Lewis, J.; Biswas, R.; Robinson, A.; Maroncelli, M. *J. Phys. Chem. B* **2001**, *105*, 3306−3318.
(47) Heitz, M. P.; Maroncelli, M. *J. Phys. Chem. A* **1997**, *101*, 5852−5868.
(48) Kordikowski, A.; Schenk, A. P.; Van Nielsen, R. M.; Peters, C. J. *J. Supercrit. Fluids* **1995**, *8*, 205−216.
(49) Brunner, E.; Hueltenschmidt, W.; Schlichthaerle, G. *J. Chem. Thermodyn.* **1987**, *19*, 273−291.
(50) Kaminishi, G. I.; Yokoyama, C.; Takahashi, S. *Fluid Phase Equilib.* **1987**, *34*, 83−99.
(51) Calculations were performed using the SUPERTRAPP program, version 3.1 (NIST Standard Reference Database 4), which employed the Peng−Robinson equation of state with van der Waals one-fluid mixing rules and the binary interaction parameter $k_{ij} = 0.109$. Such calculations provide accurate representations of the relevant properties of the *n*-pentane + CO_2 mixture as well as the pressure−composition data available for the c-C_6H_{12} + CO_2 system. From available comparisons, we anticipate errors of less than 0.05 in $x(P)$.
(52) Harris, J. G.; Yung, K. H. *J. Phys. Chem.* **1995**, *99*, 12021−12024.
(53) Jorgensen, W. L.; Madura, J. D.; Swenson, C. J. *J. Am. Chem. Soc.* **1984**, *106*, 6638−6646.
(54) Edwards, D. M. F.; Madden, P. A.; McDonald, I. R. *Mol. Phys.* **1984**, *51*, 1141−1161.
(55) Haughney, M.; Ferrario, M.; McDonald, I. R. *J. Phys. Chem.* **1987**, *91*, 4934−4940.
(56) Jorgensen, W. L.; Maxwell, D. S.; Tirado-Rives, J. *J. Am. Chem. Soc.* **1996**, *118*, 11225−11236.
(57) Stone, A. *The Theory of Intermolecular Forces*; Oxford University Press: New York, 1996.
(58) Whereas changes to repulsive interactions are needed to model solvatochromic shifts in weakly allowed transitions,[82,83] they do not appear to be necessary in the present systems.
(59) Patel, N.; Biswas, R.; Maroncelli, M. *J. Phys. Chem. B* **2002**, *106*, 7096−7114.
(60) Shalev, E.; Ben-Horin, N.; Even, U.; Jortner, J. *J. Chem. Phys.* **1991**, *95*, 3147−3166.
(61) Leontidis, E.; Suter, U.; Schutz, M.; Luthi, H.-P.; Renn, A.; Wild, U. P. *J. Am. Chem. Soc.* **1995**, *117*, 7493−7507.
(62) Kumar, P. V.; Maroncelli, M. *J. Chem. Phys.* **1995**, *103*, 3038−3060.
(63) Martins, L. R.; Skaf, M. S. *Chem. Phys. Lett.* **2003**, *370*, 683−689.
(64) Kometani, N.; Arzhantsev, S.; Maroncellli, M. *J. Phys. Chem. A* **2006**, *110*, 3405−3413.
(65) Raineri, F. O.; Friedman, H. L. *Adv. Chem. Phys.* **1999**, *107*, 81−189.
(66) Smith, W., Forester, T. R. *DL_POLY_2*, version 2.14; CCLRC Daresbury Laboratory: Daresbury, U. K., 2001.
(67) Frenkel, D.; Smit, B. *Understanding Molecular Simulation, From Algorithms to Applications*, 2nd ed.; Academic Press: New York, 2002.
(68) For simplicity, the solute volumes were assumed to be the same in all mixtures. Given that these solute volumes are <0.5% of the simulation volumes in all cases, the errors incurred by this approximation should be negligible.

(69) Reynolds, L.; Gardecki, J. A.; Frankland, S. J. V.; Horng, M. L.; Maroncelli, M. *J. Phys. Chem.* **1996**, *100*, 10337−10354.

(70) The particular reaction field factor $f(x)$ used in eq 6 is one among many possible variants.[81] Different reaction fields provide roughly the same decomposition into nuclear and electronic polarizability contributions. The main differences lie in the gas-phase frequencies that different formulations predict. In prior work on anthracene derivatives[46] we have found that the factor used in eq 6 provides a better representation of the true gas-phase frequencies than the more popular function $f(x) = (x - 1)/(2x + 1)$, and we therefore use it here.

(71) The systematic variations in the relative peak heights in the PEA emission spectra displayed in Figure 2 result from some reabsorption of the emission at the higher CH_3CN mole fractions. This effect has been accounted for when determining spectral frequencies.

(72) Biswas, R.; Lewis, J.; Maroncelli, M. *Chem. Phys. Lett.* **1999**, *310*, 485−494.

(73) Horng, M. L.; Gardecki, J. A.; Papazyan, A.; Maroncelli, M. *J. Phys. Chem.* **1995**, *99*, 17311−17337.

(74) Matyushov, D.; Newton, M. *J. Phys. Chem. A* **2001**, *105*, 8516−8532.

(75) Two different solutes were used in experiment and simulation only for convenience. We employed PEA in the experimental measurements primarily because the long ethynyl axis of this molecule enabled us to measure rotation times in addition to spectral shifts, which was not possible with anthracene. We assumed that comparing experimental shifts of PEA with simulated shifts of anthracene would be sensible based on the similarity of their $S_0 \leftrightarrow S_1$ transitions and their solvatochromism. The level of agreement achieved in the experiment−simulation comparisons observed here appears to justify this assumption.

(76) Song, W.; Maroncelli, M. *Chem. Phys. Lett.* **2003**, *378*, 410−419.

(77) Su, Z.; Maroncelli, M. *J. Chem. Phys.* **2006**, *124*, 164506.

(78) Suppan, P. *J. Photochem. Photobiol., A* **1990**, *50*, 293−330.

(79) Schulte, R. D.; Kauffman, J. F. *J. Phys. Chem.* **1994**, *98*, 8793−8800.

(80) Khajehpour, M.; Welch, C. M.; Kleiner, K. A.; Kauffman, J. F. *J. Phys. Chem. A* **2001**, *105*, 5372−5379.

(81) Koutek, B. *Collect. Czech. Chem. Commun.* **1978**, *43*, 2368−2386.

(82) Mangle, E. A.; Topp, M. R. *Chem. Phys.* **1987**, *112*, 427−442.

(83) Stratt, R. E.; Adams, J. E. *J. Chem. Phys.* **1993**, *99*, 775−788.